Progress In Electromagnetics Research B, Vol. 59, 71–87, 2014

Analysis on Strongly Coupled Oscillator Arrays Using Modified Y-Parameters Approach

Yu-Tsung Lo and Jean-Fu Kiang*

Abstract—A modified Y-parameters approach is proposed to model the behavior of coupled oscillator arrays (COA's). A coupling network with tunable coupling strength is proposed, which has a near-constant input conductance, to ensure the oscillation condition under different attenuation levels. The parameters of oscillators and the coupling network are derived on the TSMC 0.18 μm technology, and their Y parameters are extracted around 10 GHz for illustration. After being verified with full-circuit simulations and other behavior models, including the Adler's equation and the conventional Y-parameters approach, this method is applied to estimate the maximum allowable number of oscillators that can be coupled together. The inter-element phase shift of a COA is controlled by tuning the free-running frequencies of oscillators at both ends. Injection signals with proper phases are proposed to synchronize multiple COA's into a bigger COA.

1. INTRODUCTION

A coupled oscillator array (COA) can be used to supply input signals with linear phase progression to an antenna array for beam-steering or power combining [1–3]. The linear phase progression can be achieved by tuning the free-running frequencies at both ends of the array [1]; or by changing the phase difference of injection signals fed to the oscillators at both ends [4].

Locking stability of coupled oscillators has been analyzed in [5]. In [6], it is shown that the in-phase power-combining mode can be sustained by inserting a resistor at the center of the coupling network to attenuate undesired modes, or by placing two resistors at both ends of a transmission-line segment [7, 8]. In [9], an one-dimensional coupling network is proposed, which consists of one-wavelength transmission-line segments and series/shunt resistors. In [10], a non-reciprocal coupling network is used to enhance the array stability while extending the scanning range.

Bandwidth and coupling strength are two key factors in designing a coupling network. In [1], it is assumed that the Q factor of the coupling network is lower than that of the oscillators. In [11], it is pointed out that the previous assumption is not necessary if the Kurokawa's analysis [12] is applied while the oscillators and the coupling network are properly modeled in terms of the Y parameters. Hence, a narrow-band (high Q) coupling network has also been used [11].

A stronger coupling usually leads to a wider locking range [13, 14]. However, the output amplitudes of the VCO's may vary significantly under different phase progressions [7, 15]. A typical threshold between weak and strong coupling regimes, for example 0.5, has been proposed [11], around which the locking bandwidth varies significantly. With the coupling coefficient greater than 0.5, the amplitude of oscillators at both ends becomes larger than those of the interior ones [13]. Hence, there seems a trade-off between the locking bandwidth and a uniform amplitude distribution across the COA.

Several methods have been used to analyze COA's. The time evolution of frequency and phase can be obtained by solving a set of differential equations. In [8], a Y-parameters approach is used to

Received 8 January 2014, Accepted 25 March 2014, Scheduled 27 March 2014

* Corresponding author: Jean-Fu Kiang (jfkiang@ntu.edu.tw).

The authors are with the Department of Electrical Engineering and the Graduate Institute of Communication Engineering, National Taiwan University, Taipei, Taiwan.

analyze the COA's. Harmonic-balance technique has been used to derive the steady-state response of COA's [7]. In [16], a linearized discrete model is derived on the Adler's equation to study the transient behavior. In [17], two weakly coupled oscillators are analyzed using a perturbation projection vector (PPV). In [18], the steady-state amplitude and phase of two differential oscillators, coupled via a resistive network, are obtained by solving a set of differential equations.

The probability of lock tends to limit the maximum allowable size of a COA, which originates from the randomness in the free-running frequencies of the oscillators. The probability of lock decreases as the array size increases [19]. Besides, the beam-pointing error also increases with the array size [20].

In this work, a modified Y-parameters approach is proposed to simulate the behavior of a COA. A coupling network with a variable coupling strength is proposed to maintain oscillation under different attenuation levels. The parameters of the oscillators and the coupling network are designed on the TSMC 0.18 μm technology, and their Y parameters are extracted around 10 GHz for illustration. The results of this method are compared with those of the Adler's equation, the conventional Y-parameters approach, and the full-circuit simulations. The Monte-Carlo technique is introduced to this method to estimate the probability of lock due to randomness of the free-running frequencies of the oscillators. Thus, the maximum allowable number of oscillators in a COA can be estimated. We also propose to inject signals into the center oscillators of multiple COA's to synchronize them into a larger COA.

This paper is organized as follows: The modified Y-parameters approach on a COA is presented in Section 2, the designs of the proposed coupling network and VCO's are presented in Section 3, with relevant parameters extracted for numerical simulations. The fourth-order Runge-Kutta method is used to solve the differential equations. In Section 4, numerical results of different behavior models and full-circuit simulations are compared. In Section 5, the modified Y-parameters approach is applied to simulate the time evolution of instantaneous frequencies with $N > 3$, a Monte-Carlo technique is applied to simulate the randomness of free-running frequencies. A strategy of synchronizing multiple COA's is proposed and analyzed, to extend the available size of COA's. The conclusion is drawn in Section 6.

2. BEHAVIOR MODELS OF COA's

Figure 1 shows a one-dimensional coupled oscillator array (COA) of N elements, connected through an N-port coupling network. The coupling network is composed of $N-1$ modules, with each connected to two neighboring oscillators; where V_m is the voltage at port m, $Y_{\text{osc},m}$ is the output admittance of the mth oscillator, and $Y_{\text{co},m}$ is the input admittance at port m of the coupling network. The behavior of a COA has been modeled with the Y-parameters approach [8, 13], the Adler's equation; and will be modeled with a modified Y-parameters approach in this work. The COA's will be explored on their key feature of achieving linear phase progression by tuning the free-running frequencies of the oscillators at both ends.

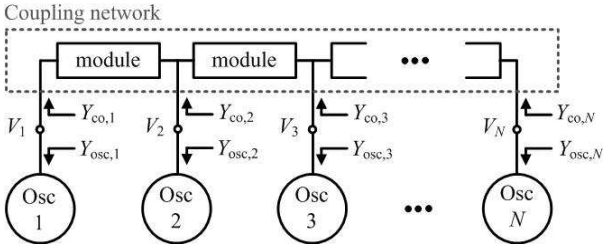

Figure 1. Coupled oscillator array (COA) connected via an N-port coupling network.

2.1. Y-Parameters Approach

The input admittance at port m of the coupling network can be represented as [4]

$$Y_{\text{co},m} = \frac{1}{V_m} \sum_{n=1}^{N} Y_{mn} V_n \tag{1}$$

where $V_m = A_m e^{j\varphi_m}$ is the voltage phasor at port m, and Y_{mn}'s are the Y parameters of the N-port coupling network. The resonance condition [21] implies that

$$Y_m\left(\omega_m, \bar{V}\right) = Y_{\text{osc},m}\left(\omega_m, V_m\right) + Y_{\text{co},m}(\omega_m, \bar{V}) = 0 \tag{2}$$

where $Y_m(\omega_m, \bar{V})$ is the total admittance at node m, and $\bar{V} = [V_1, V_2, \ldots, V_N]^t$. Although $Y_{\text{osc},m}$ and $Y_{\text{co},m}$ can be obtained independently, the free-running frequency of a stand-alone oscillator will deviate from its initial value, $\omega_{0,m}$, when connected to the coupling network.

In [8], (2) is expanded in a Taylor series around $\omega_{0,m}$ as

$$Y_m\left(\omega_{0,m}, \bar{V}\right) + \left(\omega_m - \omega_{0,m}\right) \frac{\partial Y_m(\omega_m, \bar{V})}{\partial \omega_m}\bigg|_{\omega_{0,m}} \simeq 0 \tag{3}$$

where ω_m is the instantaneous frequency. If the amplitude, A_m, and the phase, φ_m, are constant, the time derivative of $v_m(t) = \text{Re}\{A_m e^{j[\omega_{0,m}t+\varphi_m]}\}$ can be calculated as

$$\frac{d}{dt}\text{Re}\left\{A_m e^{j[\omega_{0,m}t+\varphi_m]}\right\} = \text{Re}\left\{j\omega_{0,m} A_m e^{j[\omega_{0,m}t+\varphi_m]}\right\} \tag{4}$$

If the amplitude and the phase vary slowly with time, the time derivative becomes [12]

$$\frac{d}{dt}\text{Re}\left\{A_m(t) e^{j[\omega_{0,m}t+\varphi_m(t)]}\right\} = \text{Re}\left\{j\left[\omega_{0,m} + \frac{d\varphi_m(t)}{dt} - \frac{j}{A_m(t)}\frac{dA_m(t)}{dt}\right] A_m(t) e^{j[\omega_{0,m}t+\varphi_m(t)]}\right\} \tag{5}$$

Under the condition of slow-time variation [8]:

$$\frac{d\varphi_m(t)}{dt} \ll \omega_{0,m} \quad \text{and} \quad \frac{1}{A_m(t)}\frac{dA_m(t)}{dt} \ll \omega_{0,m} \tag{6}$$

(5) can be put in the form of (4), with the instantaneous frequency, $\omega_m = \omega_{0,m} + \delta\omega_m$, where [12]

$$\delta\omega_m = \frac{d\varphi_m(t)}{dt} - j\frac{1}{A_m(t)}\frac{dA_m(t)}{dt} \tag{7}$$

Substituting (7) into (3), we obtain

$$Y_m(\omega_{0,m}, \bar{V}) + \left[\frac{d\varphi_m(t)}{dt} - j\frac{1}{A_m(t)}\frac{dA_m(t)}{dt}\right] \frac{\partial Y_m}{\partial \omega_m}(\omega_{0,m}, \bar{V}) \simeq 0 \tag{8}$$

Define an instantaneous phase, $\psi(t) = \int^t \omega_{0,m} dt + \varphi(t)$, then $d\varphi(t)/dt = d\psi(t)/dt - \omega_{0,m}$, and (8) can be reduced to [8]

$$\frac{dA_m(t)}{dt} = A_m(t)\text{Im}\left\{F_m\left(\omega_{0,m}, \bar{V}\right)\right\} \tag{9}$$

$$\frac{d\psi_m(t)}{dt} = \omega_{0,m} - \text{Re}\left\{F_m\left(\omega_{0,m}, \bar{V}\right)\right\} \tag{10}$$

where

$$F_m\left(\omega_{0,m}, \bar{V}\right) = \frac{Y_m}{\partial Y_m/\partial \omega_m}\left(\omega_{0,m}, \bar{V}\right) \tag{11}$$

The time evolution of amplitude and phase of the oscillators in a COA are governed by (9) and (10).

2.2. Adler's Equation

If the Y parameters of the coupling network is less sensitive to frequency, (9) and (10) can be reduced to the Adler's equation. If the amplitude variation is negligible, as in [1, 22], the Adler's equation can be further reduced to

$$\frac{d\psi_m}{dt} = \omega_{0,m} - \frac{\omega_{0,m}}{2Q_m}\sum_{n=1}^{N} \text{Im}\left\{\kappa_{mn}\frac{A_n}{A_m} e^{j(\psi_n - \psi_m)}\right\} \tag{12}$$

where $\kappa_{mn} = Y_{mn}/g_{pm}$ is the coupling coefficient between oscillators n and m, $Q_m = \omega_m C_m/g_{pm}$ is the quality factor of oscillator m, g_{pm} and C_m are the conductance and capacitance, respectively, of the equivalent RLC circuit representing the mth oscillator.

2.3. Modified Y-parameters Approach

In applying the conventional Y-parameters approach to analyze COA's with strong coupling [11, 13], the deviation of free-running frequencies has not been considered. Typically, an isolated VCO is designed to drive a $50\,\Omega$ load. Imagine that at $t < 0$, the mth VCO is connected to a $50\,\Omega$ load and oscillates at its designed free-running frequency, $f_{0,m}$. At $t = 0$, all the VCO's are detached from their $50\,\Omega$ loads, and switched to the coupling network.

Figure 2 illustrates the drifting of oscillation frequency $f_m^{(1)}$ from $f_{0,m}$ right after oscillators are switched to the coupling network. If $f_{0,m} > f_s$, the susceptances $B_{\mathrm{co},m}$ and $B_{\mathrm{osc},m}$ can be approximated as

$$\begin{aligned} B_{\mathrm{co},m} &= p_c \left(f_m^{(1)} - f_s \right) \\ B_{\mathrm{osc},m} &= p_o \left(f_m^{(1)} - f_{0,m} \right) \end{aligned} \tag{13}$$

where p_c and p_o are derived by curve-fitting on the simulation data of the coupling network and the mth VCO, respectively. The oscillation condition implies that $B_{\mathrm{co}} + B_{\mathrm{osc}} = 0$, which leads to

$$f_m^{(1)} = \frac{p_c f_s + p_o f_{0,m}}{p_c + p_o} \tag{14}$$

Hence, the initial frequency of the first VCO satisfies $f_s < f_1^{(1)} < f_{0,1}$. Similarly, $f_{0,N} < f_N^{(1)} < f_s$. For the other VCO's $f_m^{(1)} = f_s$ because $f_{0,m} = f_s$. Thus, we set $\omega_m^{(1)} = 2\pi f_m^{(1)}$ in (17) at the first time step.

To more accurately describe the behavior of the COA, expand (2) about the instantaneous frequency at time step n, $t = n\Delta t$, as

$$Y_m \left(\omega_m^{(n)}, \bar{V} \right) + \left(\omega_m^{(n+1)} - \omega_m^{(n)} \right) \left. \frac{\partial Y_m \left(\omega_m^{(n)}, \bar{V} \right)}{\partial \omega_m} \right|_{\omega_m^{(n)}} \simeq 0 \tag{15}$$

where $\omega_m^{(n)}$ and $\omega_m^{(n+1)}$ are the instantaneous frequencies at time steps n and $n+1$, respectively. Eqs. (9) and (10) are then modified as

$$\frac{dA_m(t)}{dt} = A_m(t) \mathrm{Im} \left\{ F_m(\omega_m^{(n)}, \bar{V}) \right\} \tag{16}$$

$$\frac{d\psi_m(t)}{dt} = \omega_m^{(n)} - \mathrm{Re} \left\{ F_m(\omega_m^{(n)}, \bar{V}) \right\} \tag{17}$$

where

$$F_m \left(\omega_m^{(n)}, \bar{V} \right) = \frac{Y_m}{\partial Y_m / \partial \omega_m} \left(\omega_m^{(n)}, \bar{V} \right) \tag{18}$$

The oscillation frequency is updated at each time step, and $\omega_m^{(n)}$ can be viewed as the free-running frequency for the next time step.

Table 1 summarizes the comparison of these three behavior models.

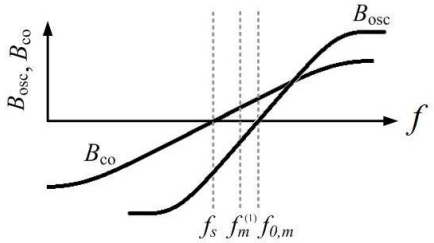

Figure 2. Adjustment of the VCO's oscillation frequency when connected to the coupling network, f_s is the target frequency, $f_{0,m}$ is the free-running frequency of the mth stand-alone oscillator, $f_m^{(1)}$ is the initial frequency of the mth oscillator after all the oscillators are connected to the coupling network.

Table 1. Comparison of behavior models.

model	modified Y-parameters approach	Y-parameters approach	Adler's equation
main idea	Taylor expansion with updated frequency	Taylor expansion	phasor diagram [22] or reduction of Y parameters [8]
key equations	$\frac{dA_m(t)}{dt}=A_m(t)\mathrm{Im}\left\{F_m(\omega_m^{(n)},\bar{V})\right\}$ $\frac{d\psi_m(t)}{dt}=\omega_m^{(n)}-\mathrm{Re}\left\{F_m(\omega_m^{(n)},\bar{V})\right\}$ where $F_m(\omega_m^{(n)},\bar{V})=\frac{Y_m}{\partial Y_m/\partial\omega_m}(\omega_m^{(n)},\bar{V})$	$\frac{dA_m(t)}{dt}=A_m(t)\mathrm{Im}\{F_m(\omega_{0,m},\bar{V})\}$ $\frac{d\psi_m(t)}{dt}=\omega_{0,m}-\mathrm{Re}\{F_m(\omega_{0,m},\bar{V})\}$ where $F_m(\omega_{0,m},\bar{V})=\frac{Y_m}{\partial Y_m/\partial\omega_m}(\omega_{0,m},\bar{V})$	$\frac{d\psi_m}{dt}=\omega_{0,m}$ $-\frac{\omega_{0,m}}{2Q_m}\sum_{n=1}^{N}\mathrm{Im}\left\{\kappa_{mn}\frac{A_n}{A_m}e^{j(\psi_n-\psi_m)}\right\}$
valid range	strong/weak coupling	strong/weak coupling	weak coupling
required parameters	Y parameters of oscillators and coupling network	Y parameters of oscillators and coupling network	coupling coefficient of coupling network and quality factor of oscillators

3. DESIGN OF COUPLING NETWORK AND VCO

3.1. Design of Coupling Network

A coupling network is designed to provide a variable coupling strength to the COA. The input conductance of the coupling network is preferred to be insensitive to the coupling strength, to make sure the negative conductance of the VCO is always sufficient to sustain the oscillation [11].

Figure 3 shows one module of the proposed coupling network, which is composed of two attenuators and a transmission-line segment of one-wavelength long. One of the attenuator is composed of transistors M_1, M_2 and M_3, the other is composed of transistors M_4, M_5 and M_6. These MOSFET's are biased in the triode region to function like a resistor. The bias voltages, V_{b1} and V_{b2}, are used to control the on-resistance of the MOSFET's, in order to adjust the insertion loss of the attenuator. By proper tuning of the bias voltages, both attenuators present a near-constant input conductance at different attenuation levels [23].

The attenuator can be modeled as a resistive T network, as shown in Figure 4, with the input impedance

$$Z_{\mathrm{in}} = R_1 + \frac{R_2(R_1+Z_0)}{R_2+R_1+Z_0} \tag{19}$$

where R_1 and R_2 are implemented with the drain-source resistance of a MOSFET. If both the source and the load are impedance-matched to Z_0, namely, $Z_{\mathrm{in}} = Z_0$, then

$$Z_0 = \sqrt{R_1^2 + 2R_1R_2} \tag{20}$$

The ratio of input to output voltages can be derived as

$$\gamma = \frac{V_i}{V_o} = \frac{R_1^2 + 2R_1R_2 + R_1Z_0 + R_2Z_0}{Z_0R_2} \tag{21}$$

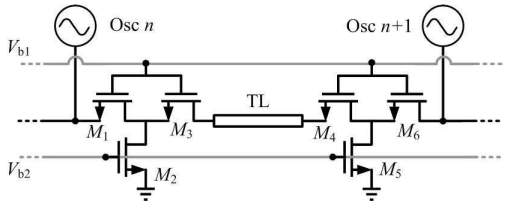

Figure 3. Module in the proposed coupling network, which is composed of two variable attenuators and one transmission-line segment.

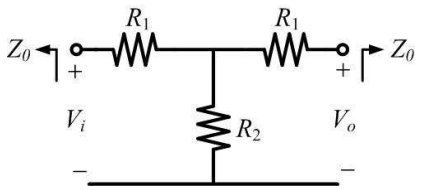

Figure 4. Equivalent T network of an attenuator.

Substituting (20) into (21), the power attenuation becomes

$$20\log_{10}\gamma = 20\log_{10}\frac{R_1+R_2+Z_0}{R_2} \tag{22}$$

A specific attenuation level, γ, can be achieved by adjusting R_1 and R_2 as

$$R_1 = Z_0\frac{\gamma-1}{\gamma+1}, \quad R_2 = Z_0\frac{2\gamma}{\gamma^2-1} \tag{23}$$

For example, to achieve 3 dB of attenuation requires $R_1 = 8.5\,\Omega$ and $R_2 = 142\,\Omega$, under $Z_0 = 50\,\Omega$.

The $ABCD$ matrix of the T network is

$$\begin{bmatrix} A & B \\ C & D \end{bmatrix} = \begin{bmatrix} 1+R_1/R_2 & 2R_1+R_1^2/R_2 \\ 1/R_2 & 1+R_1/R_2 \end{bmatrix} \tag{24}$$

By cascading the $ABCD$ matrices of the two attenuators and the one-wavelength transmission-line with phase constant β and physical length ℓ, the $ABCD$ matrix of one module in the coupling network can be derived and transformed to a Y matrix

$$\bar{\bar{Y}}_s = \begin{bmatrix} Y_{11,s} & Y_{12,s} \\ \\ Y_{21,s} & Y_{22,s} \end{bmatrix}$$

where

$$\begin{aligned}
Y_{11,s} &= \frac{(BC+A^2)\cos\beta\ell + j(ACZ_0+ABY_0)\sin\beta\ell}{(BA+AB)\cos\beta\ell + j(A^2Z_0+B^2Y_0)\sin\beta\ell} \\
Y_{21,s} &= -\frac{1}{(BA+AB)\cos\beta\ell + j(A^2Z_0+B^2Y_0)\sin\beta\ell} \\
Y_{12,s} &= \frac{(A^4+B^2C^2)(\cos^2\beta\ell-\sin^2\beta\ell) - 2A^2BC}{(BA+AB)\cos\beta\ell + j(A^2Z_0+B^2Y_0)\sin\beta\ell} \\
Y_{22,s} &= \frac{(A^2+BC)\cos\beta\ell + j(ACZ_0+ABY_0)\sin\beta\ell}{(BA+AB)\cos\beta\ell + j(A^2Z_0+B^2Y_0)\sin\beta\ell)}
\end{aligned} \tag{25}$$

The Y parameters of the N-port coupling network can be expressed in terms of the Y parameters in (25) as

$$Y_{mn} = \begin{cases} Y_{11,s}, & m=n=1,N \\ 2Y_{11,s}, & m=n\neq 1,N \\ Y_{12,s}, & |m-n|=1 \\ 0, & \text{otherwise} \end{cases} \tag{26}$$

Figure 5 shows the Y-parameters of the proposed coupling network. The results using (26) match well with those using the Agilent ADS simulation tools with the TSMC 0.18 µm circuit models, over the band of 5–15 GHz. The difference between the results using (26) and those with the circuit simulation tools is attributed to the parasitics of the transistors, which are not taken into account in the former.

Figure 6 shows the simulated drain-source resistances, $R_{1,\mathrm{ds}}$ and $R_{2,\mathrm{ds}}$, of transistors M_1 and M_2, respectively. Specific attenuation level can be achieved by proper adjustment of R_1 and R_2 by (23), via control voltages, V_{b1} and V_{b2}, respectively. For example, to tune the attenuation from 3 to 10 dB, one needs to adjust R_1 from 8.5 to 26 Ω and R_2 from 142 to 35 Ω. The widths of M_1 and M_2 are 256 µm and 42 µm, respectively, working under a bias voltage from 0 to 1.8 V.

Figure 7(a) shows the simulated attenuation of the attenuator at 10 GHz. The attenuation level of 3 to 10 dB can be achieved by controlling the bias voltages, V_{b1} and V_{b2}. Relevant parameters are listed in Table 2. Figure 7(b) shows the input resistance and coupling coefficient of a module under different attenuation levels. Note that the total attenuation provided by a module is 2γ, and the input resistance is kept close to 50 Ω. Compared to the purely resistive coupling circuit in [24, 25], our coupling network is designed to maintain a near-constant input conductance to ensure oscillation at different attenuation levels.

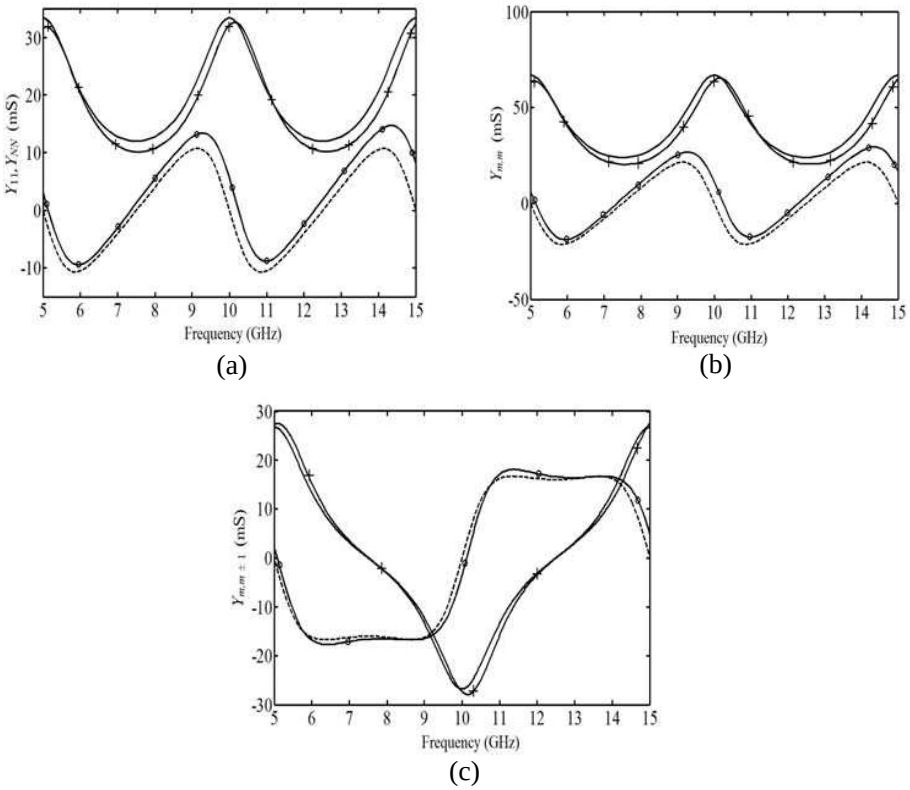

Figure 5. Y-parameters of the proposed N-port coupling network at $\gamma = 3\,\text{dB}$, ——: $\text{Re}\{Y_{mn}\}$ using (26), $-+-$: $\text{Re}\{Y_{mn}\}$ using circuit simulation, $---$: $\text{Im}\{Y_{mn}\}$ using (26), $-\circ-$: $\text{Im}\{Y_{mn}\}$ using circuit simulation; (a) $m = n = 1, N$, (b) $m = n \neq 1, N$, (c) $|m - n| = 1$.

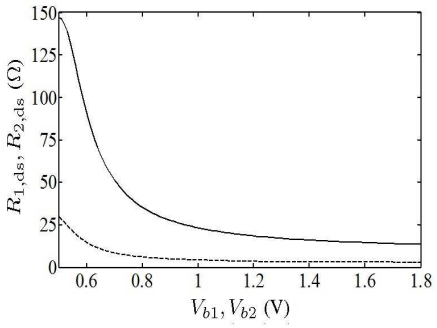

Figure 6. Simulated drain-source resistances: (a) $R_{1,\text{ds}}$ (controlled by V_{b1}) and (b) $R_{2,\text{ds}}$ (controlled by V_{b2}).

The coupling coefficient between oscillators n and m can be defined as [8]

$$\kappa_{mn} = \frac{Y_{mn}}{g_{pm}}, \quad |m - n| = 1 \tag{27}$$

where Y_{mn} is listed in (26), and g_{pm} is the conductance of the equivalent RLC circuit representing the mth oscillator. Figure 7(b) shows the relation between the coupling coefficient and the attenuation level, with the frequency close to 10 GHz. As mentioned in [11], $\kappa_{mn} > 0.5$ implies a strong coupling, and $\kappa_{mn} < 0.5$ implies a weak coupling. The coupling coefficient is about 0.5 at the attenuation level of 9 dB.

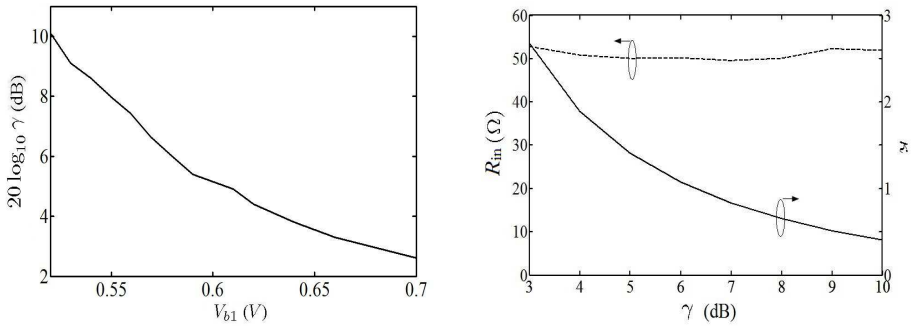

Figure 7. Simulated (a) attenuation and (b) input resistance and coupling coefficient, of the attenuator at 10 GHz.

Table 2. Parameters to achieve desired attenuation levels.

γ (dB)	3	4	5	6	7	8	9	10
R_1 (ω)	8.6	11.3	14	16.6	19.1	21.5	23.8	26
V_{b1} (V)	0.7	0.64	0.61	0.58	0.56	0.55	0.53	0.52
$R_{1,\mathrm{ds}}$ (Ω)	8.4	11.3	13.6	16.9	19.6	21.2	24.6	26.4
R_2 (Ω)	142	105	82.2	66.9	55.8	47.3	40.6	35
V_{b2} (V)	0.53	0.58	0.62	0.65	0.68	0.72	0.75	0.8
$R_{2,\mathrm{ds}}$ (Ω)	139	104.2	80	66.5	56.5	46.9	41.7	35.3

If the coupling network is only slightly dependent on the frequency within the band of interest, a coupling coefficient can be conveniently defined to model it [8]. Stronger coupling usually leads to stronger frequency dependence of the coupling network [13]. The frequency-dependent Y parameters can be used to model the proposed coupling network over the band of interest more accurately, when solving (9) and (10) [13], or solving (16) and (17).

3.2. Design of VCO

Figure 8 shows the schematic of the VCO adopted in this work, which is designed to operate around 10 GHz. Its free-running frequency can be tuned by applying the control voltage, V_{ctrl}, to the RF MOS varactors, C_1 and C_2, to tune over a range from 0.66 pF to 0.91 pF. The two inductors of the LC circuit are implemented with a 1-turn transformer in the TSMC models, with radius of 110 µm. The width/length (w/ℓ_t) of transistors M_2 and M_3 are 80/0.18, and is 70/0.18 of transistor M_1, the bias current source. The quality factor of the LC circuit is about 10. The phase noise is -95 dBc/Hz at 1 MHz offset and -100 dBc/Hz at 1.5 MHz offset, with $V_{\mathrm{ctrl}} = 1$ V. The total dc current is 5.6 mA and the supply voltage is 1.2 V. The free-running frequency of the oscillator can be tuned from 9.5 to 12.3 GHz as V_{ctrl} is adjusted in the range of 0 to 1.8 V.

The oscillator can be modeled as an RLC circuit connected to an active device, as shown in Figure 9. For the mth oscillator, the free-running frequency is $\omega_{0,m} \simeq 1/\sqrt{L_m C_m}$. The output admittance can be expressed as

$$Y_{\mathrm{osc},m} = G_{\mathrm{osc},m} + jB_{\mathrm{osc},m} \tag{28}$$

where $G_{\mathrm{osc},m} = g_{pm} - g_{am}$, and $-g_{am}$ is the negative conductance provided by the cross-couple pair.

By the van der Pol equation [1, 26], g_{am} is related to the oscillation amplitude, A_m, as [27, 28]

$$g_{am}(A_m) = -g_1 + 3g_2 A_m^2 \tag{29}$$

where g_1 and g_2 are empirical coefficients. Thus, we have

$$G_{\mathrm{osc},m}(A_m) = g_{pm} - \left(-g_1 + 3g_2 A_m^2\right) \tag{30}$$

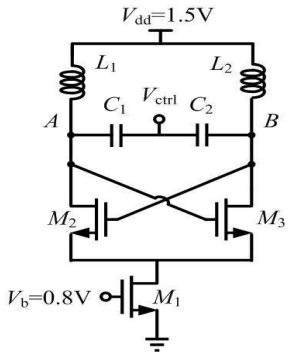

Figure 8. Schematic of VCO used in the COA.

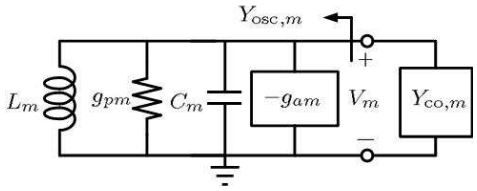

Figure 9. Schematic of a parallel *RLC* circuit connected to an active device and a coupling network.

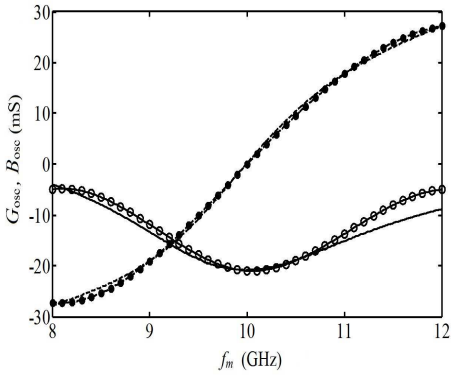

Figure 10. Output admittance of oscillator m with $A_m = 75\,\text{mV}$, ——: simulated $G_{\text{osc},m}$, − − −: simulated $B_{\text{osc},m}$, −○−: curve-fitted $G_{\text{osc},m}$, −●−: curve-fitted $B_{\text{osc},m}$.

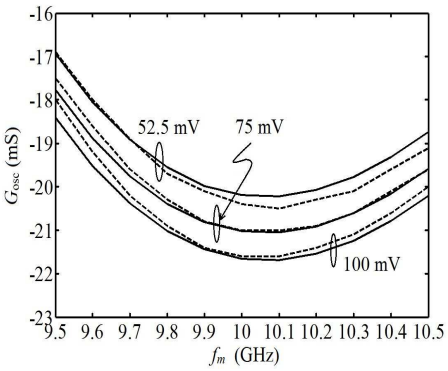

Figure 11. Output conductance of oscillator m with different amplitudes, $f_{0,m} = 10\,\text{GHz}$, ——: simulation with ADS, − − −: curve-fitting with (31).

The oscillation amplitude can be tuned by adjusting the bias current of the oscillator. Using the ADS simulation tools, we obtain $G_{\text{osc},m}(0.0525) = -0.02\,\text{S}$, $G_{\text{osc},m}(0.075) = -0.021\,\text{S}$, and $G_{\text{osc},m}(0.1) = -0.0218\,\text{S}$; where the oscillation amplitude falls within the range of 52.5 to 100 mV.

Note that $G_{\text{osc},m}$ must be less than $-0.02\,\text{S}$ to drive the coupling network with input resistance of $50\,\Omega$. With $g_{pm} = 0.01\,\text{S}$, it is required that $g_{am}(0.0525) = 0.03\,\text{S}$, $g_{am}(0.075) = 0.031\,\text{S}$, and $g_{am}(0.1) = 0.0318\,\text{S}$. By fitting values of A_m between 52.5 and 100 mV in (29), using the least mean-square-error method, we derive $g_1 = -0.029$ and $g_2 = 0.119$.

The frequency response of Y_{osc} in (30) can be fitted with third-order polynomials as

$$\begin{aligned} G_{\text{osc},m}(f_m, A_m) &\simeq g_{pm} - g_{am}(A_m) + a\left(f_m - f_m^{(1)}\right) + b\left(f_m - f_m^{(1)}\right)^2 + c\left(f_m - f_m^{(1)}\right)^3 \\ B_{\text{osc},m}(f_m) &\simeq p(f_m - f_m^{(1)}) + q\left(f_m - f_m^{(1)}\right)^2 + r\left(f_m - f_m^{(1)}\right)^3 \end{aligned} \tag{31}$$

where $f_m^{(1)}$ and f_m (in GHz) are the initial frequency and the instantaneous frequency, respectively, of the mth VCO. Table 3 lists the coefficients, a, b, c, p, q and r, at different free-running frequencies, by curve-fitting Y_{osc} using the least mean-square-error method. Figure 10 shows the output admittance of oscillator m, with the amplitude of 75 mV.

Figure 11 shows the output conductance, G_{osc}, at a finer resolution, with the amplitude of 52.5, 75 and 100 mV, respectively. The variation of circuit parameters with amplitude and frequency has been incorporated.

Table 3. Coefficients in $Y_{\text{osc},m}$ at different free-running frequencies.

$f_m^{(1)}$ (GHz)	9.6	9.7	9.8	9.9	10	10.1	10.2	10.3	10.4
$10^3 \times a$	2.7	1.8	0	−1.2	−3.2	−3.7	−4.1	−6.2	−7
$10^3 \times b$	6.6	8.0	9.0	10.8	11.8	11.8	11.9	11.0	10.5
$10^3 \times c$	−2.5	−2.9	−3.2	−3.7	−3.7	−3.6	−3.6	−2.8	−2.5
$10^3 \times p$	21.3	21.6	21.7	21.7	21.3	21.2	21	19.9	19.4
$10^3 \times q$	−8.0	−7.3	−6.5	−4.2	−1.3	0	0	3.8	4.9
$10^3 \times r$	1.8	1.5	1.1	0	−1.0	−1.3	−1.6	−2.8	−3.2

4. VERIFICATION OF MODIFIED *Y*-PARAMETERS APPROACH

For comparison, the transient response of a three-element ($N = 3$) COA is simulated with the modified Y-parameters approach, the Y-parameters approach, the Adler's equation, and the ADS full-circuit simulation. The governing equations of the three different behavior models are solved using the fourth-order Runge-Kutta method.

The free-running frequencies of the oscillator at both ends are tuned to $f_s + \Delta f_0$ and $f_s - \Delta f_0$, respectively; where f_s is the target frequency of 10 GHz, Δf_0 is a specific frequency offset selected to achieve the desired phase progression. The free-running frequencies of the other oscillators are tuned to f_s.

The stability of a system can be checked by perturbing its amplitude and phase, then examining whether such perturbation will decay as time marches [1]. To find the sufficient condition of stability, the Jacobian matrix associated with (9) and (10) can be derived [8], then checked if its eigenvalues have negative real part [29].

An alternative to examine the stability of the COA is to observe its transient response, which converges to a steady state if the COA is stable [30]. In this work, the stability condition is checked by observing the time evolution of amplitude and phase in the numerical solution. When the COA is successfully locked, the amplitudes and phases of oscillators always converge. If the COA fails to lock, the instantaneous frequency of each oscillator wobbles around its free-running frequency, the amplitudes and phases also wobble without convergence.

Figure 12 shows the time evolution of instantaneous frequency and phase difference of a three-element COA, with $\gamma = 5$ dB and $\Delta f_0 = 400$ MHz, and Y_{osc} is modeled with (31). All three oscillators are locked into a single frequency, but slightly deviated from the planned 10 GHz. This deviation is due to the asymmetry of Y_{osc} about the center frequency of 10 GHz, and can be corrected using injection-locking [31] or phase-locked loop (PLL) technique [32].

Figure 13 shows the effect of Δf_0 on the phase difference, using the Adler's equation, the Y-parameters approach, the modified Y-parameters approach, the ADS simulation, and an estimation formula in (A6). It is observed that weaker coupling induces larger phase difference, at a given Δf_0.

The Adler's equation fails to predict the phase difference, θ, under strong coupling, possibly because the amplitude variation is not considered, as in (12). A modified Adler's equation, including amplitude variation, can be found in [14]. It also indicates that using the coupling coefficient and the quality factor may not be sufficient to model the COA's behavior. The formula in (A6) does not include the amplitude and frequency dependence of the transconductance, hence only provides a rough estimation. The predictions with the Y-parameters approach match reasonably well with the ADS simulation when Δf_0 is small. However, as Δf_0 increases, a large difference appears between the Y-parameters approach and the ADS simulation. The results of the modified Y-parameters approach match well with the ADS simulation when Δf_0 is small, and the difference with the ADS simulation at large Δf_0 is smaller compared to the conventional Y-parameters approach.

The modified Y-parameters approach is more accurate than the other two behavior models, and takes much shorter simulation time than the ADS full-circuit simulation. Hence, the modified Y-

parameters approach is an effective and efficient way to simulate large COA's. Combining with the Monte-Carlo technique, it can be used to simulate the random frequency distribution of oscillators, which causes phase error and sometimes a loss of lock in a COA. Besides, the instantaneous frequencies of the oscillators can be directly observed. Figure 14 summarizes the flow-chart of applying this approach.

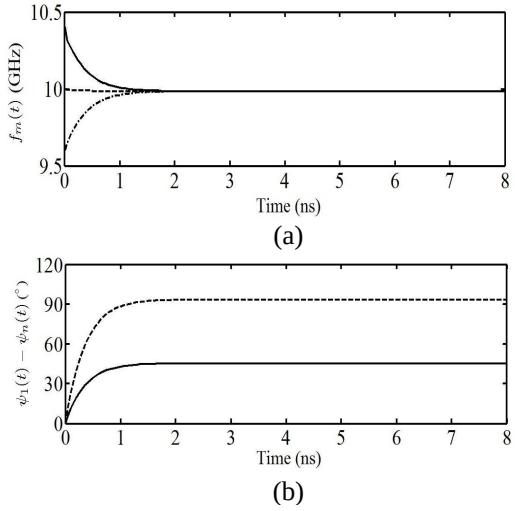

Figure 12. Time evolution of (a) instantaneous frequency (——: $f_1(t)$, − − −: $f_2(t)$, − · −: $f_3(t)$), and (b) phase difference (——: $\psi_1 - \psi_2$, − − −: $\psi_1 - \psi_3$) of the three-element COA, $\gamma = 5\,\text{dB}$, $\Delta f_0 = 400\,\text{MHz}$, Y_{osc} is modeled with (31).

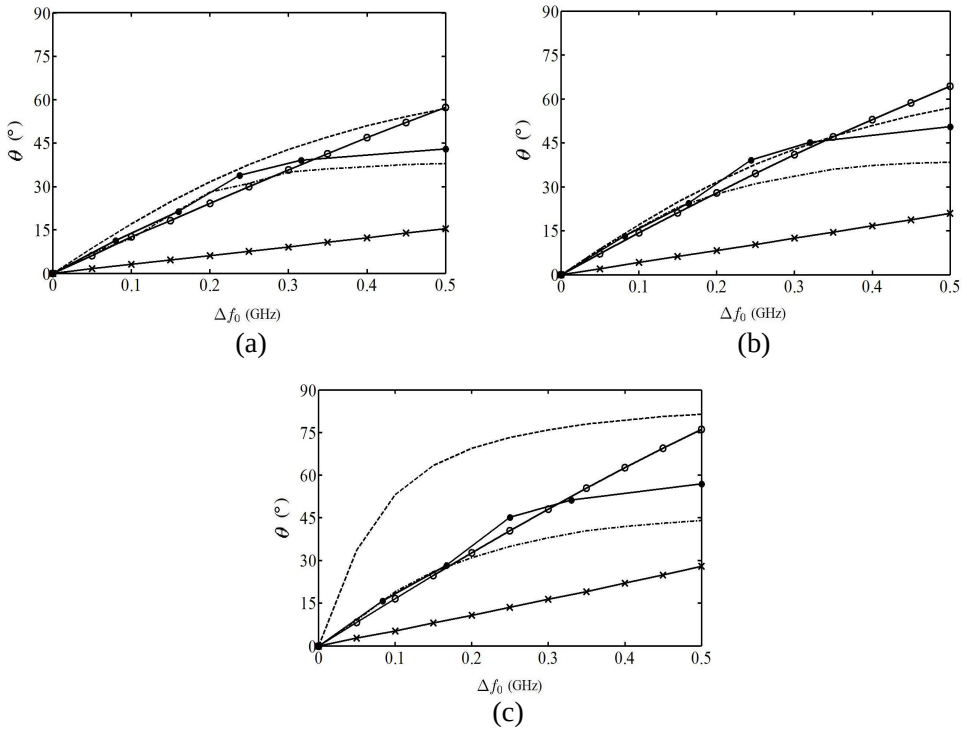

Figure 13. Inter-element phase difference of a three-element COA, under different free-running frequency offsets, Δf_0, —●—: modified Y-parameters approach (16) and (17), —○—: Y-parameters approach (9) and (10), —×—: Adler's Eq. (12), − · −: ADS simulation, − − −: estimation with (A6), (a) $\gamma = 4\,\text{dB}$, (b) $\gamma = 5\,\text{dB}$, (c) $\gamma = 6\,\text{dB}$.

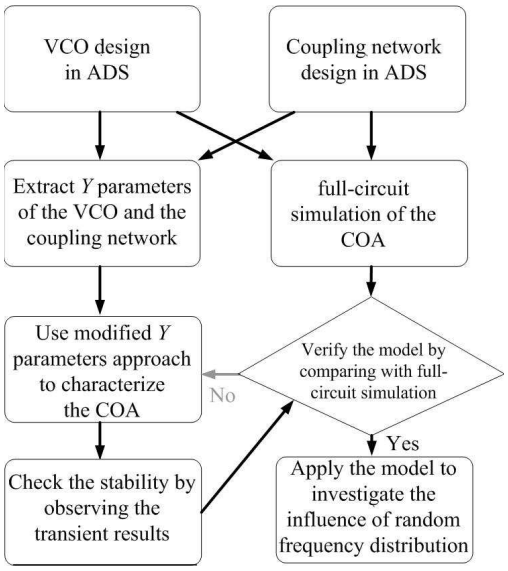

Figure 14. Flow-chart of applying the modified Y-parameters approach.

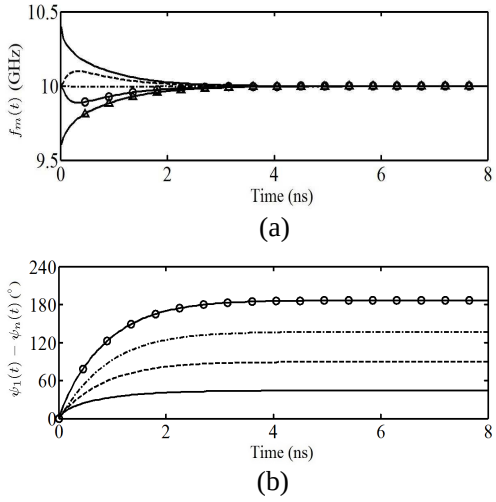

Figure 15. Time evolution of (a) instantaneous frequencies (——: $f_1(t)$, $-\,-\,-$: $f_2(t)$, $-\cdot-$: $f_3(t)$, $-\circ-$: $f_4(t)$, $-\Delta-$: $f_5(t)$), and (b) phase differences (——: $\psi_1-\psi_2$, $-\,-\,-$: $\psi_1-\psi_3$, $-\cdot-$: $\psi_1-\psi_4$), $-\circ-$: $\psi_1-\psi_5$) of a five-element COA, $\gamma = 5\,\text{dB}$, $\Delta f_0 = 400\,\text{MHz}$, Y_{osc} is modeled with (31).

5. SYNCHRONIZATION OF MULTIPLE COA's

Figure 15(a) shows the time evolution of instantaneous frequencies of a five-element COA, with $f_s = 10\,\text{GHz}$, $\gamma = 5\,\text{dB}$ and $\Delta f_0 = 400\,\text{MHz}$. The free-running frequencies of the first and the last VCO's are set to $f_s + \Delta f_0$ and $f_s - \Delta f_0$, respectively; and those of the other three VCO's are set to f_0 [1, 8].

As the COA's are switched to the coupling network, the frequency of the second VCO is pulled upwards by the first one, and that of the fourth VCO is pulled downwards by the fifth one. After a while, the second VCO is pulled downwards and the fourth VCO is pulled upwards. Finally, all the VCO's synchronize themselves and lock into the same frequency. The associated phase differences are shown in Figure 15(b), and it appears that the inter-element phase shift is close to a constant.

In [33], the harmonic-balance technique is applied to simulate COA's of size $3 \le N \le 6$, with coupling resistors of $100\,\Omega$ and $300\,\Omega$. It appears that the inter-element phase difference is almost independent of N. Figure 16 shows the inter-element phase difference with $2 \le N \le 11$. The phase difference at $\Delta f_0 = 400\,\text{MHz}$ is larger than that at $\Delta f_0 = 100$. At smaller offset frequency, Δf_0, or stronger coupling (lower γ), the inter-element phase difference is less sensitive to N. As the coupling becomes weaker or the offset frequency increases, the inter-element phase difference tends to decrease with N.

5.1. Randomness of Free-running Frequencies

In practice, the free-running frequencies of all the VCO's bear certain randomness, which may prevent the VCO's from locking into one another, especially when the array size is large. The maximum tolerable frequency deviation due to randomness has been discussed in [1, 19]. The variation of free-running frequency depends on the process, the temperature, the stability of supply voltages, and the configuration of oscillator array. In [34], the free-running frequency of a ring oscillator array can be self-calibrated within a standard deviation, 2.79% of the center frequency at 1.3 GHz. In [35], the maximum frequency deviation of a VCO at 1 GHz is about 500 kHz, derived by measuring the spectrum over 30 seconds. In [6], the average oscillation frequency of 12.45 GHz is reported to have a maximum deviation of 15 MHz.

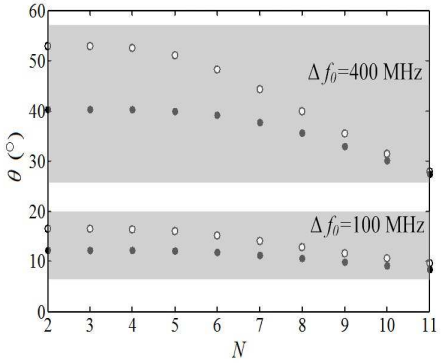

Figure 16. Inter-element phase difference, θ (°), of COA's with size N, •: $\gamma = 4\,\text{dB}$, ○: $\gamma = 6\,\text{dB}$.

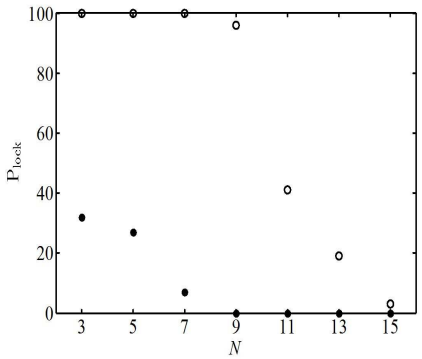

Figure 17. Probability of lock, $\sigma = 5\,\text{MHz}$, $\Delta f_0 = 200\,\text{MHz}$, ○: $\gamma = 5\,\text{dB}$, •: $\gamma = 6\,\text{dB}$.

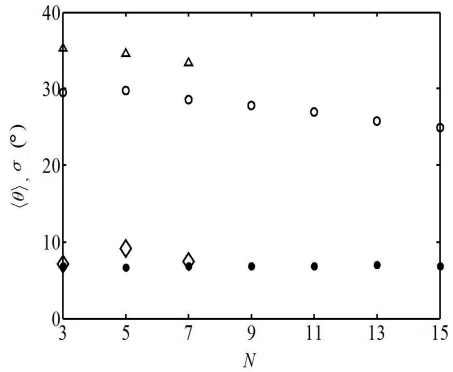

Figure 18. Average and standard deviation of phase difference, $\sigma = 5\,\text{MHz}$ and $\Delta f_0 = 200\,\text{MHz}$. •: σ at $\gamma = 5\,\text{dB}$, ◇: σ at $\gamma = 6\,\text{dB}$, ○: $\langle\theta\rangle$ at $\gamma = 5\,\text{dB}$, △: $\langle\theta\rangle$ at $\gamma = 6\,\text{dB}$.

Assume the free-running frequencies of the VCO's in the COA follow a normal distribution, with the mean value of 10 GHz and a standard deviation of $\sigma_0 = 5\,\text{MHz}$. By applying the Monte-Carlo technique, the free-running frequency of each VCO is simulated as a random variable. For an N-element COA, N random variables are required in the behavior models, and a total of 5000 realizations are implemented. In each realization, the Runge-Kutta solver is applied to trace the time evolution of the instantaneous frequencies and phases. The COA may be locked or not, contingent upon the distribution of free-running frequencies; It is claimed locked if the steady-state frequencies of all the VCO's are different by less than $\sigma_0/5$. We choose $\sigma_0/5$ as the locking criterion because Y_{osc} is modeled with 2001 data points from 9 to 11 GHz, rendering a frequency resolution of 1 MHz.

Figure 17 shows the probability of lock, P_{lock}, which is the number ratio of Monte-Carlo realizations when the COA is locked to the total number of realizations. The probability of lock decreases as N is increased or as the attenuation level is increased. A stronger coupling strength is required to achieve a higher probability of lock. The proposed variable-coupling network with near-constant input conductance is capable of supporting large COA's. A coupling network made of resistors may quench the oscillation under strong coupling because the resistive loss is not compensated for by the transistors.

Figure 18 shows the mean phase difference, $\langle\theta\rangle$, and the standard deviation, σ, derived from the Monte-Carlo realizations with successful locking. The frequency offset of the two end VCO's is set to $\Delta f_0 = 200\,\text{MHz}$, which falls within the valid range of the behavior models, as shown in Figure 13. It is observed that a higher attenuation level leads to a larger average phase difference and a slight increase of standard deviation.

5.2. Synchronization by Phase Injection

To extend the size of a COA when the random deviation of free-running frequencies is considered, one may consider a concatenation of multiple sub-COA's of smaller size. However, two sub-COA's

are generally locked into different phases, although a phase progression can be established among the oscillators within each sub-COA. An injection signal is proposed to feed the center element of each sub-COA to create phase synchronization among different sub-COA's. Figure 19 shows the schematic of two sub-COA's fed with the same injection signal, but at different phases. The equation governing the center oscillator is modified to

$$\frac{d\psi_m(t)}{dt} = \omega_m^{(n)} - \mathrm{Re}\left\{F_m(\omega_m^{(n)}, \bar{V})\right\}, \quad m \neq N_c \tag{32}$$

$$\frac{d\psi_m(t)}{dt} = \omega_m^{(n)} - \mathrm{Re}\left\{F_m(\omega_m^{(n)}, \bar{V})\right\} + \frac{\omega_{0,m}\kappa}{2Q}\sin(\psi_{\mathrm{inj}} - \psi_m(t)), \quad m = N_c \tag{33}$$

where ψ_{inj} is the phase of the injection signal, $N_c = (N+1)/2$ with N an odd number without loss of generality, κ the coupling coefficient defined in (27), and Q the quality factor of the resonant circuit. The first two terms on the right-hand side of (33) account for the mutual coupling with the modified Y-parameters approach, the third term accounts for the injection locking with the Adler's equation. A similar equation to (32) and (33) can be found in [36], in which the injection signal is fed to the end elements, the mutual coupling and the injection locking mechanism are modeled with the Adler's equation.

Consider an example as shown in Figure 19. In each sub-COA, let $N = 11$, $f_s = 10\,\mathrm{GHz}$, $\Delta f_0 = 150\,\mathrm{MHz}$, and $\gamma = 4\,\mathrm{dB}$, which implies $\kappa = 1.89$ from Figure 7(b). As f is close to f_s, (31) implies that the admittance of the resonant circuit is $Y_{pm} = g_{pm} + jp(f_m - f_{0,m})$, where $p = 0.02$, and f in units of GHz. The resonant circuit with $Y_p = g_p + j4\pi C(f - f_0)$ has a Q factor of $Q = 2\pi f_0 C/g_p$ [37]. Hence, $p = 4\pi \times 10^9 \times C$. If $g_p = 0.01$, then $Q = 10$.

By substituting $\kappa = 1.89$ and $Q = 10$ into (32) and (33), both sub-COA's turn out to synchronize in frequency and phase. To establish a contiguous phase progression from one sub-COA to the other,

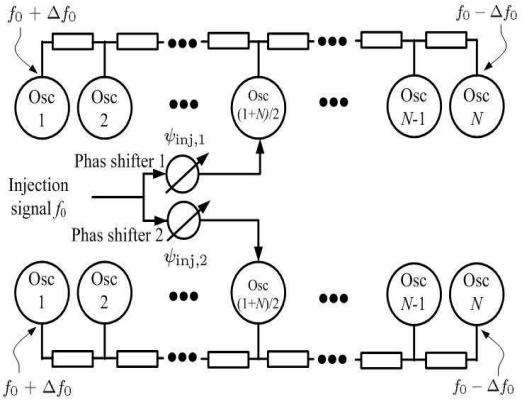

Figure 19. Schematic of two sub-COA's fed by injection signals with different phases.

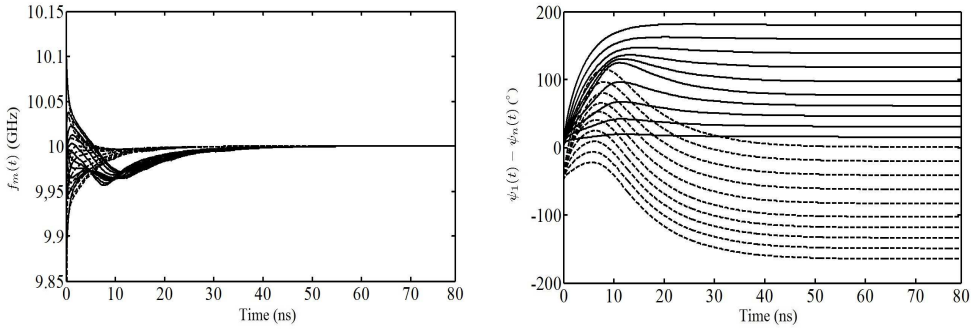

Figure 20. Time evolution of two 11-element sub-COA's with a common injection signal to the center element of each sub-COA, $f_{\mathrm{inj}} = 10\,\mathrm{GHz}$, $\psi_{\mathrm{inj},1} = 0°$, $\psi_{\mathrm{inj},2} = 180°$. Both COA's operate with $\Delta f_0 = 150\,\mathrm{MHz}$ and $\gamma = 4\,\mathrm{dB}$.

we set $\psi_{\text{inj},1} = 0^\circ$ and $\psi_{\text{inj},2} = (N-1)\theta$, where θ is the inter-element phase shift within each sub-COA.

Figure 20 shows the time evolution of frequencies and phases of two 11-element sub-COA's, synchronized with $\psi_{\text{inj},1} = 0^\circ$ and $\psi_{\text{inj},2} = 180^\circ$, respectively. The inter-element phase shift turns out to be around 18°. Both sub-COA's are locked to the same desired frequency of 10 GHz, and their phases progress linearly from one sub-COA to the other, doubling the total length of the COA. More sub-COA's can be synchronized with injection signals of proper phases to achieve a much longer COA with linear phase progression.

6. CONCLUSION

A modified Y-parameters approach is proposed to simulate the behavior of COA's. A variable-coupling network with near-constant input conductance is designed to maintain oscillation under different coupling strengths. The proposed approach has been verified with full-circuit simulations, and compared with the conventional Y-parameters approach and the Adler's equation. Monte-Carlo technique has been applied to simulate random deviation of free-running frequencies, which tends to reduce the probability of lock as the array size is increased. A phase-injection method is also proposed to synchronize multiple COA's into an effectively larger COA.

ACKNOWLEDGMENT

This work was sponsored by the National Science Council, Taiwan, R.O.C., under contract NSC 101-2221-E-002-129.

APPENDIX A. RELATION BETWEEN INTER-ELEMENT PHASE DIFFERENCE AND FREE-RUNNING FREQUENCY OFFSET

In the steady state, the voltage phasors of a three-element COA satisfy

$$\begin{bmatrix} Y_{11,s}+Y_{\text{osc},1} & Y_{12,s} & 0 \\ Y_{12,s} & 2Y_{11,s}+Y_{\text{osc},2} & Y_{12,s} \\ 0 & Y_{12,s} & Y_{11,s}+Y_{\text{osc},3} \end{bmatrix} \begin{bmatrix} V_1 \\ V_2 \\ V_3 \end{bmatrix} = 0 \tag{A1}$$

where $V_n = A_n e^{j\psi_n}$ is the voltage phasor at port n. The voltages, V_1 and V_3, can be solved in terms of V_2 as

$$\begin{bmatrix} Y_{11,s}+Y_{\text{osc},1} & -(Y_{11,s}+Y_{\text{osc},3}) \\ Y_{12,s} & Y_{12,s} \end{bmatrix} \begin{bmatrix} V_1 \\ V_3 \end{bmatrix} = \begin{bmatrix} 0 \\ -(2Y_{11,s}+Y_{\text{osc},2})\,V_2 \end{bmatrix} \tag{A2}$$

with the explicit solutions

$$\begin{aligned} V_1 &= C\,(Y_{11,s}+Y_{\text{osc},3}) \\ V_3 &= C\,(Y_{11,s}+Y_{\text{osc},1}) \end{aligned} \tag{A3}$$

where

$$C = \frac{-(2Y_{11,s}+Y_{\text{osc},2})\,V_2}{Y_{12,s}\,(2Y_{11,s}+Y_{\text{osc},1}+Y_{\text{osc},3})} = C_r e^{j\psi_c}$$

Let $f_{0,1} = f_s + \Delta f_0$ and $f_{0,3} = f_s - \Delta f_0$. Eq. (31) is simplified to have $Y_{\text{osc},1} \simeq g_{p1} - g_{a1} + jp(f_1 - f_{0,1})$ and $Y_{\text{osc},3} \simeq g_{p3} - g_{a3} + jp(f_3 - f_{0,3})$. The values of p at $f_{0,1}$ and $f_{0,3}$ are approximately the same, as listed in Table 3. When the three oscillators are locked, $f_1 = f_3 = f_s$, we have $g_{p1} - g_{a1} \simeq g_{p3} - g_{a3} = g = -0.0215$. Hence, (A3) can be reduced to

$$\begin{aligned} A_1 e^{j\psi_1} &= C_r e^{j\psi_c}\,\{G_{11,s} + g + j[B_{11,s} + p(f_s - f_{0,3})]\} \\ A_3 e^{j\psi_3} &= C_r e^{j\psi_c}\,\{G_{33,s} + g + j[B_{33,s} + p(f_s - f_{0,1})]\} \end{aligned} \tag{A4}$$

where $Y_{11,s} = G_{11,s} + jB_{11,s}$, $G_{11,s} = G_{33,s}$ and $B_{11,s} = B_{33,s}$.

Due to symmetry of the COA and the coupling network with respect to the center oscillator, $A_1 = A_3 = A_0$ and $B_{11,s} = B_{33,s} \simeq 0$, hence (A4) can be further reduced to

$$\begin{aligned} A_1 e^{j\psi_1} &= A_0 e^{j(\psi_c+\theta)} \\ A_3 e^{j\psi_3} &= A_0 e^{j(\psi_c-\theta)} \end{aligned} \tag{A5}$$

where

$$\begin{aligned} A_0 &= C_r \sqrt{(G_{11,s}+g)^2 + (p\Delta f_0)^2} \\ \theta &= \tan^{-1} \frac{p\Delta f_0}{G_{11,s}+g} \end{aligned} \tag{A6}$$

which an explicit relation between the inter-element phase difference, θ, and the free-running frequency offset, Δf_0.

REFERENCES

1. York, R. A., "Nonlinear analysis of phase relationships in quasi-optical oscillator arrays," *IEEE Trans. Microwave Theory Tech.*, Vol. 41, No. 10, 1799–1809, Oct. 1993.
2. Neff, J. D., B. K. Meadows, E. A. Brown, S. P. DeWeerth, and P. Hasler, "A CMOS coupled nonlinear oscillator array," *IEEE Int. Symp. Circ. Syst.*, Vol. 4, IV-301–IV-304, 2002.
3. Tousi, Y. M., O. Momeni, and E. Afshari, "A novel CMOS high-power terahertz VCO based on coupled oscillators: Theory and implementation," *IEEE J. Solid-State Circuits*, Vol. 47, No. 12, 3032–3042, Dec. 2012.
4. Stephan, K. D. and W. A. Morgan, "Analysis of inter-injection-locked oscillators for integrated phased arrays," *IEEE Trans. Antennas Propagat.*, Vol. 35, No. 7, 771–781, Jul. 1987.
5. Lynch, J. J. and R. A. York, "Stability of mode locked states of coupled oscillator arrays," *IEEE Trans. Circuits Syst. I*, Vol. 42, No. 8, 413–418, Aug. 1995.
6. Nogi, S., J. Lin, and T. Itoh, "Mode analysis and stabilization of a spatial power combining array with strongly coupled oscillators," *IEEE Trans. Microwave Theory Tech.*, Vol. 41, No. 10, 1827–1837, Oct. 1993.
7. Georgiadis, A., A. Collado, and A. Suarez, "New techniques for the analysis and design of coupled-oscillator systems," *IEEE Trans. Microwave Theory Tech.*, Vol. 54, No. 11, 3864–3877, Nov. 2006.
8. York, R. A., P. Liao, and J. J. Lynch, "Oscillator array dynamics with broadband N-port coupling networks," *IEEE Trans. Microwave Theory Tech.*, Vol. 42, No. 11, 2040–2045, Nov. 1994.
9. Pogorzelski, R. J., "On the design of coupling networks for coupled oscillator arrays," *IEEE Trans. Antennas Propagat.*, Vol. 51, No. 4, 794–801, Apr. 2003.
10. Martinez-Lopez, J. I., R. Moussounda, and R. G. Rojas, "Non-reciprocal coupling network for beam-steering coupled oscillator arrays," *IET Microwave Antennas Propagat.*, Vol. 5, No. 8, 940–947, 2011.
11. Lynch, J. J. and R. A. York, "Synchronization of oscillators coupled through narrow-band networks," *IEEE Trans. Microwave Theory Tech.*, Vol. 49, No. 2, 237–249, Feb. 2001.
12. Kurokawa, R., "Injection locking of microwave solid-state oscillators," *Proc. IEEE*, Vol. 61, No. 10, 1386–1410, Oct. 1973.
13. Seetharam, V. and L. W. Pearson, "Analysis of strong coupling in coupled oscillator arrays," *IEEE Trans. Antennas Propagat.*, Vol. 58, No. 4, 1067–1075, Apr. 2010.
14. Jiang, H. and R. Penno, "Effects of amplitude dynamics on beam steering and shaping in coupled oscillator array," *IEEE Antennas Wireless Propagat. Lett.*, Vol. 9, 474–477, 2010.
15. Herran, L. F., S. V. Hoeye, M. Fernandez, C. Vazquez, and F. L. Heras, "Analysis of phase distribution errors in mutually coupled harmonic self-oscillating mixers," *IEEE Trans. Microwave Theory Tech.*, Vol. 57, No. 12, 2853–2861, Dec. 2009.

16. Pogorzelski, R. J., "Generalization of the linearized discrete model of coupled oscillator arrays to account for coupling delay," *Radio Sci.*, Vol. 43, RS4070, 2008.
17. Maffezzoni, P., "Synchronization analysis of two weakly coupled oscillators through a PPV macromodel," *IEEE Trans. Circuits Syst. I*, Vol. 57, No. 3, 654-663, Mar. 2010.
18. Ionita, M., D. Cordeau, J. M. Paillot, S. Bachir, and M. Iordache, "A CAD tool for an array of differential oscillators coupled through a broadband network," *Int. J. RF Microwave Computer-Aided Eng.*, Vol. 23, No. 2, 178–187, 2013.
19. Strogatz, S. H. and R. E. Mirollo, "Phase-locking and critical phenomena in lattices of coupled nonlinear oscillators with random intrinsic frequencies," *Physiza D*, Vol. 33, 143–168, 1988.
20. Shen, J. and L. W. Pearson, "The phase error and beam-pointing error in coupled oscillator beam-steering arrays," *IEEE Trans. Antennas Propagat.*, Vol. 53, No. 1, 386–393, Jan. 2005.
21. Vendelin, G. D., A. M. Pavio, and U. L. Rohde, *Microwave Circuit Design Using Linear and Nonlinear Techniques*, 384–391, Wiley-Interscience, 1990.
22. Adler, R., "A study of locking phenomena in oscillators," *Proc. IRE, Waves Electrons*, Vol. 34, 351–357, Jun. 1946.
23. Ellinger, F., *Radio Frequency Integrated Circuits and Technologies*, 385–387, Springer, 2007.
24. Martineau, B., O. Richard, N. Rolland, A. Cathelin, and A. Kaiser, "A 20–23 GHz coupled oscillators array in 65 nm CMOS for HDR 60 GHz beamforming applications," *Euro. Solid State Circuit Conf.*, 463–466, Helsinki, Finland, Sep. 2011.
25. Lopez, J., D. Y. C. Lie, B. K. Meadow, and J. Cothern, "Fully-integrated 1-dimensional RF coupled-oscillator network for phase-shifterless phased array systems," *IEEE Bipolar/BiCMOS Circuit Tech. Meeting*, 17–20, Portland, Oregon, USA, Oct. 2010.
26. Van der Pol, B., "The nonlinear theory of electric oscillations," *Proc. IRE*, Vol. 22, 1051–1085, Sep. 1934.
27. Humphrey, D. E. J., V. F. Fusco, and S. Drew, "Active antenna array behavior," *IEEE Trans. Microwave Theory Tech.*, Vol. 43, No. 8, 1819–1825, Aug. 1995.
28. Cordeau, D., M. Ionita, J. M. Paillot, and M. Iordache, "New formulation of the equations describing the locked states of two Van der Pol oscillators coupled through a broadband network — Application to the design of two differential coupled VCOs," *Freq. J. RF — Eng. Telecommun.*, Vol. 67, Nos. 7–8, 237–247, 2013.
29. Jordan, D. W. and P. Smith, *Nonlinear Ordinary Differential Equations*, 4th Edition, Chapter 8, Oxford University Press, 2007.
30. Pogorzelski, R. J. and A. Georgiadis, *Coupled-oscillator Based Active-array Antennas*, Chapter 8, John Wiley, 2012.
31. Collado, A. and A. Georgiadis, "Performance of coupled-oscillator arrays with angle-modulated injection signals," *IEEE Trans. Circuits Syst. I*, Vol. 7, No. 9, 2343–2352, Sep. 2010.
32. Yan, S. H. and T. H. Chu, "A beam-steering antenna array using injection locked coupled oscillators with self-tuning of oscillator free-running frequencies," *IEEE Trans. Antennas Propagat.*, Vol. 56, No. 9, 2920–2928, Sep. 2008.
33. Suarez, A., F. Ramirez, and S. Sancho, "Stability and noise analysis of coupled-oscillator systems," *IEEE Trans. Microwave Theory Tech.*, Vol. 59, No. 4, 1032–1046, Apr. 2011.
34. Zhang, X., I. Mukhopadhyay, R. Dokania, and A. B. Apsel, "A 46-μW self-calibrated gigahertz VCO for low-power radios," *IEEE Trans. Circuit Syst. II*, Vol. 58, No. 12, 847–851, Dec. 2011.
35. "Boosting PLL design efficiency, from free-running VCO characterizations to closed-loop PLL evaluations," Appl. Note, http://cp.literature.agilent.com/litweb/pdf/5989-9848EN.pdf.
36. York, R. A. and T. Itoh "Injection and phase-locking techniques for beam control," *IEEE Trans. Microwave Theory Tech.*, Vol. 46, No. 11, 1920–1929, Nov. 1998.
37. Collin, R. E., *Foundations for Microwave Engineering*, 2nd edition, 327, McGraw-Hill, Inc., 1992.